Indian Journal of Chemistry
Vol. 63, October 2024, pp. 945-958
DOI: 10.56042/ijc.v63i10.10916

Computational studies and *in silico* evaluation of Cd (II) and Zn (II) complexes revealing their anti-cancer trait

Maithra Nagaraju[a], Arijit Das*[b], Paresh Debnath[b], Chethan Burudeghatta Sundaramurthy[a,c] & Neratur Krishnappagowda Lokanath*[a]

[a] Department of Studies in Physics, University of Mysore, Mysuru 570 006., India
[b] Department of Chemistry, Bir Bikram Memorial College, Agartala 799 004, West Tripura, India
[c] Department of Basic Science, Amruta Institute of Engineering and Management Sciences, Bidadi, Bengaluru 572 109, India
E-mail: arijitdas78chem@gmail.com, lokanath@physics.uni-mysore.ac.in

Received 6 May 2024; accepted (revised) 23 September 2024

Computational studies offer to explore mechanistic aspects of molecular interactions with the potential to deliver practical strategies and enable rational *in silico* drug design. New powerful cancer drugs are crucial, as evidenced by the prevalence of extensively and multi-drug-resistant tuberculosis. This research work describes the use of DFT for the optimization of zinc and cadmium metal complexes. FMO distribution and its based electronic properties, and electrostatic potential have been studied. According to ADMET analysis, every substance is safe for biological use and non-carcinogenic. Both complexes have been docked to human-GTPase-K-Ras protein to determine binding ability and modes. The stability of protein-drug complexes has been probed through MD simulations, focusing on the most tightly bound complex. The Zn-complex is more thermodynamically stable compared to Cd-complex. Good ligand binding interaction with the receptor protein has been identified through molecular docking analysis mainly because of non-bonding interactions. Finally, these results might help develop a novel anti-cancer agent.

Keywords: Cd(II) and Zn(II) complexes, Computational studies, DFT, Molecular docking studies, Anti-cancer mannerism

In the current year, Das *et al.*[1] synthesized Cd(II) and Zn(II) complexes of 2-mercaptopyridine $[Cd(2\text{-}mcpH)_4](NO_3)_2$ and $[Zn(2\text{-}mcpH)_4](NO_3)_2$ due to the diverse applications of metal complexes, the synthesis and computational studies of these complexes have been in high trend[2,3]. Nitrogen-containing ligands form versatile complexes with cadmium and zinc, serving as catalysts and contributing to luminescent materials across various applications[4–6] due to their fascinating structure and feasibility in their conformations. The coordination environment *i.e.* the type of the ligand determines the complexes properties. Therefore, the theoretical analysis of these complexes will yield important insights into the metal centre's coordination preferences and the complexes' confirmation[7,8]. It has been reported that the metal complexes exhibit excellent inhibitory actions[9,10]. Zinc and cadmium metal complexes featuring multidentate ligands have garnered attention for their applications in photocatalysis, photoluminescence, and fluorescence sensing, targeting both organic and inorganic analytes[11–13].

Exploring the diverse characteristics of metal complexes involving cadmium and zinc is crucial due to their significant roles in numerous biochemical processes. Zinc has long been recognized as a crucial component of enzymes involved in metabolic processes. However, the perception of cadmium as highly toxic and biologically harmful has dominated scientific understanding[14, 15]. Recently, attention has shifted towards studying cadmium complexes due to their emerging significance in biological systems. This interest has been spurred by the invention of a carbonic anhydrase enzyme in the marine diatom *Thalassiosira weissflogii*, where cadmium has been found in active site[15].

Recent advancements in the synthesis of metal-based complexes have opened avenues for novel therapeutic approaches, particularly in combating medication resistance and toxicity associated with platinum-containing complexes[16]. Notably, a mixed ligand Zn(II) complex incorporating 1-phenyl-3-methyl-4-acyl-5-pyrazolones has exhibited promising cytotoxic activity against DUI45, LNCaP, and PC-3 human prostate cancer cells, positioning them as viable alternatives to platinum (II) complexes in the

development of antitumor drugs[17]. Additionally, the growth of MCF-7 human breast cancer cells has been demonstrated to be dose-dependently inhibited by zinc (II) complexes featuring bis-benzimidazole derivatives[18]. Further investigations into the anticancer potential of metal complexes have explored the efficacy of Zn(II) and Cd(II) complexes with various ligands, including curcumin[19], substituted nitro phenol Schiff base[20], and benzyl pyridine thiosemicarbazone derivatives[21–23], shedding light on their mechanisms of action and therapeutic implications.

However, a growing area of chemistry research aims to comprehend how different supramolecular assemblies are constructed using non-covalent interactions as the binding forces. By doing so, one can modify the characteristics of complexes to suit certain applications. The exploration of cadmium-based complexes has undergone a transformation, driven by their significance in both biological contexts and the development of molecular materials[24,25].

In recent years, computational investigations have been utilized extensively to support the conclusions drawn from experiments[26]. Further, the computational analysis helps in the investigation of various electronic and chemical related properties of the molecular system such as the ionization energy, HOMO-LUMO energy gap, absorption behaviour, corrosion inhibition[27–29], *etc*.

In this present study, we have carried out the evaluation of various properties of the synthesized zinc and cadmium-based metal complexes[1]. Alternatively, researchers have employed computational techniques such as density functional theory (DFT) computations to study the electronic characteristics of these complexes. Further, intrigued by the findings, the inhibition activity of these complexes was explored using computational tools such as molecular docking and molecular dynamics studies against 4TQ9 protein.

Materials and methods

Quantum computational studies

For over a decade, quantum computational techniques have been pivotal in theoretically exploring the physicochemical properties of compounds. Using the B3LYP functional with a 6-311+G(d,p) mixed basis set, we optimized structures of metal complexes. Visualizing the highest occupied molecular orbitals (HOMO) and lowest unoccupied molecular orbitals (LUMO) through frontier molecular orbital analysis (FMO) provided insights into their electronic properties. Utilizing Koopmans' approximation, we calculated the energy difference and various local and global molecular parameters, elucidating the chemical characteristics of the synthesized complexes. To discern charge distribution and identify reactive sites, molecular electrostatic potential (MEP) analysis was conducted. Additionally, natural bond orbital (NBO) analysis was employed to investigate different interaction types contributing to molecular structure stabilization. All computations were carried out by using the Gaussian 16 package, and the results were visualized using GaussView 6.0.16 software[30–32].

Additionally, Bader's quantum theory of atoms in molecules (QTAIM) was used, facilitating a quantum mechanical examination of the complexes' structures. By identifying bond critical points (BCPs) and bond paths, this approach offered a visual representation of noncovalent interactions within the complexes, aiding in the prediction of bond strength and nature. Moreover, the analysis utilized reduced density gradient (RDG) to characterize non-covalent interactions (NCI) and electron localized function (ELF) maps to visualize regions of high electron pair probability densities. These analyses were conducted using Multiwfn 3.8 software, with output results examined and analyzed through the visual molecular dynamics (VMD) 1.9.3 tool[33].

ADMET analysis

The intestinal absorption and brain access of the novel complexes were analysed through boiled-Egg model of Swiss ADME online tool[34]. Further, the drug-likeness of the Cd and Zn complexes are comprehended with the help of pkCSM online tool[35], which also provided the quantitative results Absorption, Distribution, Metabolism, Excretion and Toxicity (ADMET) of the complexes.

Molecular docking analysis

The synthesized complexes were subjected to molecular docking against the protein with PDB ID of 4TQ9 which is a G12V oncogenic mutant of human GTPase K-Ras protein which revealed their anti-cancer trait. The GTPase known as K-Ras facilitates cellular signalling and the stimulation of cellular proliferation, growth, survival, and

differentiation[36]. Further, between an active GTP bound and an inactive GDP bound state, the 4TQ9 protein acts as a molecular switch[37,38]. Continuous signalling networks which are related with oncogenic cellular growth are triggered by mutant K-Ras-GTP[39–41]. Hence, the inhibition of this protein will aid in the treatment of the cancer.

To understand the interaction and inhibiting ability of the novel Cd and Zn complex against G12V oncogenic mutant of human GTPase K-Ras protein molecular docking was performed. The 4TQ9 protein was extracted from RCSB PDB site, which is then converted into protein.pdb file using Biovia Discovery Studio software[42]. Autodock Tools[43] in combination with Autodock Vina[44] and Autodock 4.2[43,45] is used to obtain protein.pdbqt and ligand.pdbqt files. Further, the molecular docking process employs Autodock Vina software, wherein a three-dimensional grid box is generated with specified grid size (X= 94, Y= 98, Z= 100 for Cd complex and X= 94, Y= 88, Z= 104 for Zn complex) and grid centre (X= –5.667, Y= –23.389, Z= 46.694 for Cd complex and X= –4.694, Y= –22.528, Z= 44.778 for Zn complex) is considered. The visualization of the protein-complex and its 2D interactions are carried out using Biovia Discovery studio software.

Molecular dynamics simulation

To explore the stability of ligand-protein binding, researchers conducted a molecular dynamics (MD) simulation study using the Desmond modules within the Schrödinger 2020-22 suite[46]. The best pose of docking having highest binding affinity was selected for the MD simulation. The processed protein-ligand complex (.pdb) format was utilized in Schrodinger's protein preparation wizard, water molecules were removed and to optimize the complex OPLS3 force field was used.

Further, the energy minimized protein-complex was solvated using TIP3P water model with single point charge using orthorhombic box shape boundary conditions. Then the optimized system was neutralized using Na^+ and Cl^- ions. The protein-ligand complex underwent a 100-nanosecond relaxation period within a system set at 1 bar pressure and 300 Kelvin temperature using a barostat and thermostat, respectively. This analysis occurred within the NPT (number of atoms, constant pressure, and constant temperature) ensemble. The stability assessment utilized RMSD (Root Mean Square Deviation) and RMSF (Root Mean Square Fluctuation) plots[47,48].

Results and Discussion

Density functional theory analysis

The synthesized Cd and Zn complexes underwent optimization of molecular geometry employing density functional theory (DFT), utilizing the B3LYP correlation functional with a 6-311+G(d,p) basis set for non-metal atoms and LANL2DZ for metal atoms. Fig. 1 illustrates the optimized geometric arrangement of the complexes in their ground state. The absence of the negative frequencies confirmed the achievement of the true local minima of the geometry of the complexes. This optimized structure is further used for the other theoretical calculations.

Frontier molecular orbital analysis

The molecular orbitals distribution of the two highest HOMOs and LUMOs of the Cd and Zn

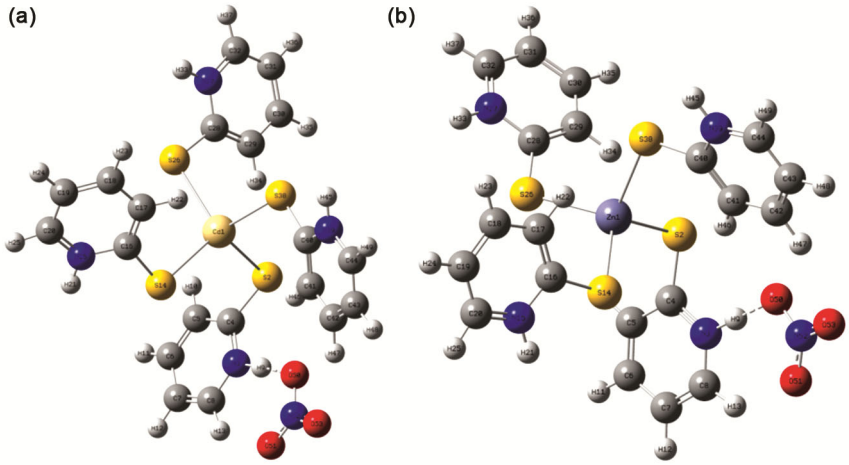

Fig. 1 — Optimized molecular structures of (a) Cd and (b) Zn complex, respectively

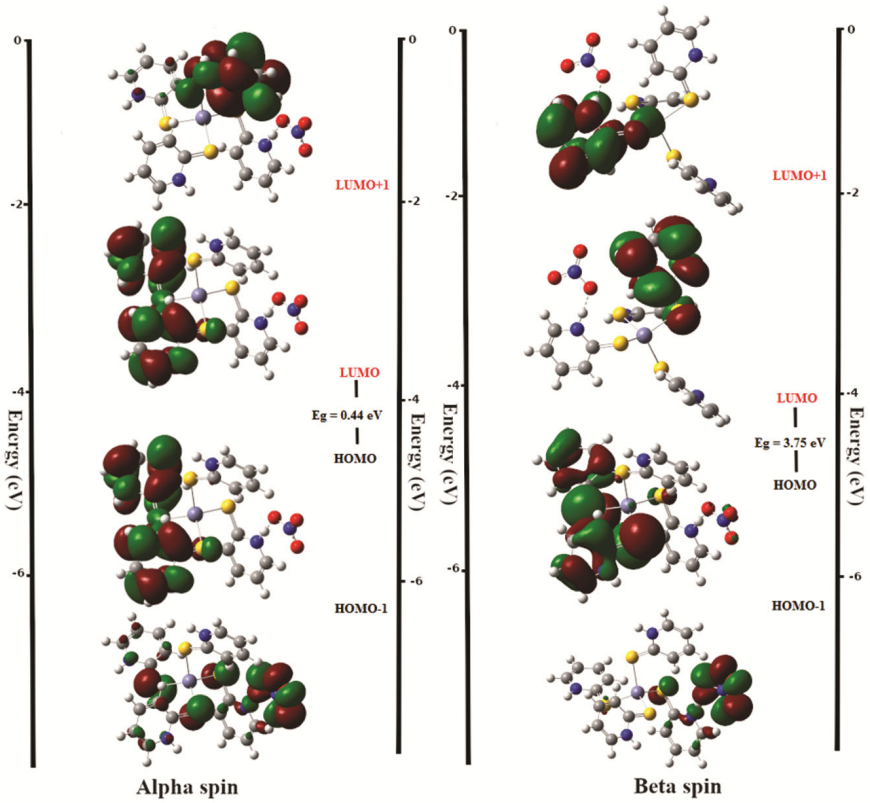

Fig. 2 — The molecular orbital profile of Cd complex with an energy level diagram

complexes are plotted to examine the variation in electron density distribution and hence to determine the possibility of the molecules to interact with other reactants. Using the E_{HOMO} and E_{LUMO} various other global and local properties such as E_{HOMO}-E_{LUMO} energy gap (ΔE), electron affinity (A), ionization energy (I), electro negativity (χ), global hardness (η), chemical potential (μ), and global softness (σ) were obtained. These reactive descriptors of the synthesized metal complexes derived from the conceptual density functional theory helps us to get better insight towards the structure, stability, and global chemical reactivity.

The orbital arrangement of Cd and Zn complexes are shown in the Fig. 2 and Fig. 3, respectively. It is observed that for the Cd complex, the molecular orbitals are highly occupied. In contrast, for the Zn complex, the orbitals are shown to be uniformly distributed. The energy differences of 0.4414 eV and 3.7462 eV are observed for α and β molecular orbitals of the Cd complex, respectively. On the other hand, the HOMO-LUMO energy gap for alpha (α) and beta (β) molecular orbitals of the Zn complex are found to be 0.4860 eV and 3.7345 eV, respectively. The values of all the molecular parameters of both the complexes are found to be comparable with each other. The electron affinities of both the complexes reveal that they act as electron acceptors, thus they actively take part in the intramolecular charge transfer (ICT). The calculated energy values of the molecular orbitals and the corresponding electronic properties of both complexes of Zn(II) and Cd(II) are given in the Table 1.

Molecular electrostatic potential (MEP) analysis

The MEP map derived from the electron density distribution, offers a graphical representation elucidating potential active sites within molecules. This visualization aids in comprehending the molecules' chemical reactivity profiles effectively. In addition to this, it also revealed the directionality of the nucleophilic and electrophilic attack. The colour scheme ranges from –0.08496 a.u. to 0.08496 a.u. and –0.08547 a.u. to 0.08547 a.u. for Cd and Zn complexes, respectively. The colour scheme used in the MEP map helps in visualizing the nucleophilic (negative potential) and electrophilic centers (positive potential) indicated by red and blue colours, respectively. The intermediate electrostatic potential falls in the order: blue > green > yellow > orange > red, as depicted in Fig. 4, which showcases MEP

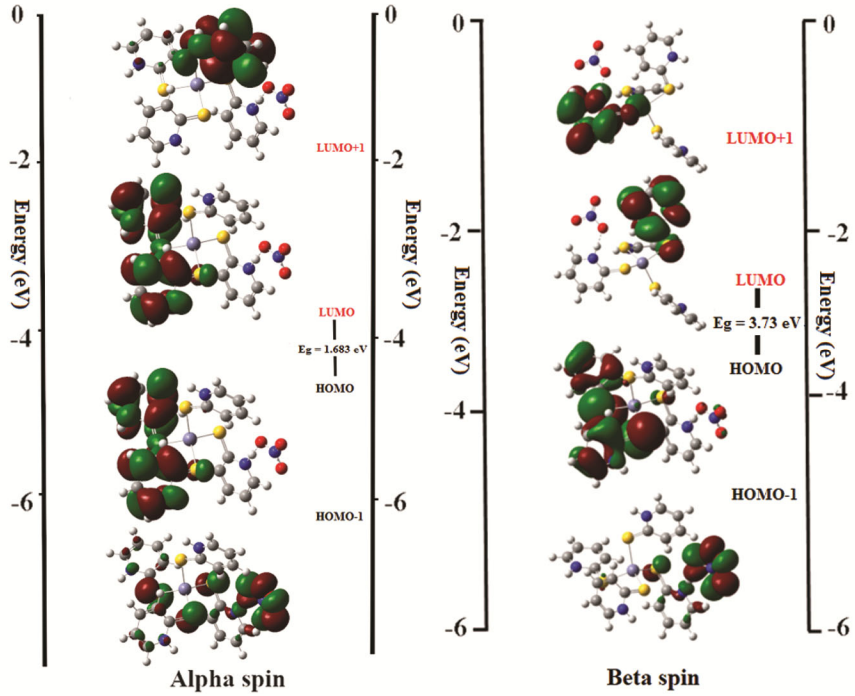

Fig. 3 — The molecular orbital distribution on the Zn complex with an energy level diagram.

Table 1 — Tabulation of the various electronic properties related to Cd and Zn complexes.

Electronic properties	Cd complex		Zn complex	
	Alpha spin	Beta spin	Alpha spin	Beta spin
E_{HOMO} (eV)	–2.9195	–5.9427	–2.9386	–5.9264
E_{LUMO} (eV)	–2.4781	–2.1965	–2.4526	–2.1919
HOMO-LUMO energy gap (ΔE) (eV)	0.4414	3.7462	0.4860	3.7345
Ionization energy (I) (eV)	2.9195	5.9427	2.9386	5.9264
Electron affinity (A) (eV)	2.4781	2.1965	2.4526	2.1919
Electronegativity (χ) (eV)	2.6988	4.0696	2.6956	4.0591
Chemical potential (μ) (eV)	–2.6988	–4.0696	–2.6956	–4.0591
Global hardness (η) (eV)	0.2207	1.8731	0.2430	1.8672
Global softness (s) (eV)	4.5314	0.5339	4.1153	0.5355
Electrophilicity index (ω) (eV)	16.5024	4.4209	14.9509	4.4120

maps for both complexes, each with its respective scale.

Natural bond orbital (NBO) analysis

The NBO analysis helped in examining the nature and type of the chemical bonds formed, and thus to understand the stability of the compounds. It also provided information regarding various kinds of interactions associated with the compounds such as inter and intramolecular interactions, delocalization of electron density, hyper-conjugation, and all possible interactions between the acceptor and the donor natural bond orbitals. The greater second-order stabilization energies ($E^{(2)}$) observed in these complexes suggest a stronger degree of conjugation, primarily attributed to the significant electron donation from the donors to the acceptor.

In addition to this, the NBO studies also revealed the hyper-conjugative interactions formed by the overlap of orbitals between LP(3)(O53) → π*(C51–N52) and LP*(1)(C20) → π*(C18–C19) with the stabilization energies 97.44 and 49.07 kcal/mol, respectively for Cd complex, and LP(3)(O53) → π*(C51–N52) and LP*(1)(C20) → π*(C18–C19) with the stabilization energies 121.89 and 49.14 kcal/mol, respectively for Zn complex, leading to the stabilization of the complexes because of the intramolecular charge transfer. The interactions

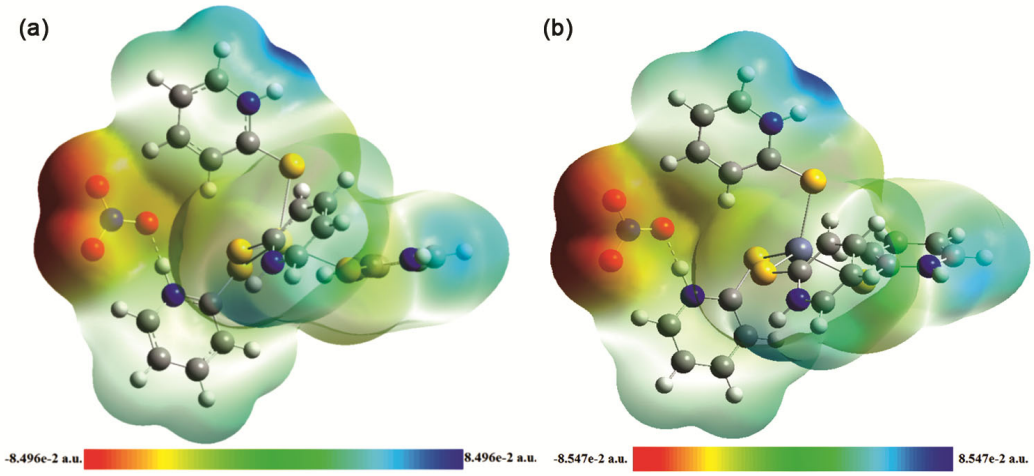

Fig. 4 — MEP plots of (a) Cd and (b) Zn complex

between the lone pair (LP(1) and LP(2)) atoms and the anti-bonding acceptor (π* and σ*) atoms also contribute towards the stabilization energies of the complexes. The major interaction energies of possible intensive interactions are provided in Table 2.

Topology analysis

The strength and nature of chemical bonds were predicted by the QTAIM studies. The critical points and bond paths within molecular structures help us think about the non-covalent contacts present in those molecules. By analysing these points, we can determine various properties of these interactions, such as electron density ($\rho(r)$), Laplacian of the electron density ($\nabla^2\rho(r)$), electron kinetic ($G(r)$), electronic potential ($V(r)$), ellipticity of the electron density ($\epsilon(r)$) and total energy densities ($H(r)$). These calculations were conducted for both the complexes under study. Further, these parameters helped in predicting the character of the chemical bonds formed.

In both the complexes, the $\rho(r)$ and $|V(r)|/G(r)$ are found to be < 1 indicating the non-covalent interactions to be weak electrostatic in nature. Further, the small positive values of $\epsilon(r)$ and $H(r)$ at the BCPs (N3-H9…. O58 and N3-H9…. O58 for Cd and Zn complexes, respectively) indicated the electron delocalization at the particular bonds and the closed-shell interactions respectively (Fig. 5). The QTAIM properties of the metal complexes are provided in Table 3.

RDG based NCI analysis

The NCI analysis using RDG was conducted to gain insights into the intramolecular interactions linked with the metal complexes. There are various kinds of interactions present in the complexes that are specified by the colour-filled RDG based iso-surfaces: strong hydrogen bond interactions are identified by the blue regions, the green region represents van der Walls interaction, and the steric interactions are attributed by the red regions. In addition to this, the two-dimensional scatter plots were generated to examine the strength of the non-covalent interactions exhibited by the complexes.

The 2D scatter plots of the complexes along with their coloured peaks corroborate the 3D iso surface plot. For the Cd complex, the blue coloured peaks observed in the range –0.02 a.u. to –0.05 a.u. indicates the strong attractive interaction, whereas the red spikes observed in the range 0.01 a.u. to 0.05 a.u. indicates the steric repulsion and the green coloured peak observed at –0.01 a.u. associates with the van der Waals type of interactions. Further, in the 2D scatter plot of Zn complex the blue coloured peaks observed in the region –0.025 a.u. to 0.05 a.u. indicating the strong attractive interactions, whereas, the red and green coloured peaks were found to be observed at 0.01 a.u. to 0.05 a.u. and –0.01 a.u. to 0.01 a.u., respectively.

The 3D NCI isosurface and 2D scatter graphs of both the complexes are shown in the Fig. 5 and Fig. 6 respectively.

ELF analysis

The ELF analysis sheds light on the intricate connection between a molecule's structure and its electron density distribution. Utilizing ELF as a surface analysis tool, we gain insight into the molecular zones with a heightened probability of

Table 2 — Tabulation of the interaction energies calculated based on the NBO analysis for both (a) Cd and (b) Zn complexes.

(a)

Type	Occupancy	Donor atoms (i)	Type	Occupancy	Acceptor atoms (j)	E(2) kcal/ mol
LP (3)	0.74935	O53	π*	0.36686	O51 - N52	97.44
LP*(1)	0.58785	C20	π*	0.00671	C18 - C19	49.07
LP (3)	0.84661	O50	π*	0.36686	O51 - N52	46.16
LP (1)	0.84051	N15	LP*(1)	0.58785	C20	38.36
LP (1)	0.60766	C30	π*	0.17649	C28 - C29	36.31
LP (1)	0.60766	C30	π*	0.13908	C31 - C32	33.23
π*	0.12035	C43 - C44	π*	0.09564	C41 - C42	27.35
π*	0.27709	N3 - C4	π*	0.12713	C5 - C6	26.65
LP (3)	0.82771	S2	LP*(6)	0.25608	Cd1	25.52
LP (3)	0.84012	S38	π*	0.32169	N39 - C40	25.2
π	0.84318	C18 - C19	LP*(1)	0.58785	C20	22.56
LP (3)	0.8587	S14	LP*(6)	0.25608	Cd1	21.84
LP (2)	0.93183	O50	σ*	0.05485	N3 - H9	20.65
π	0.81864	C41 - C42	π*	0.32169	N39 - C40	19.9
π*	0.27709	N3 - C4	π*	0.12611	C7 - C8	19.29
π*	0.32169	N39- C40	π*	0.09564	C41 - C42	18.11
LP (3)	0.85726	S26	LP*(6)	0.25608	Cd1	18.09
LP (1)	0.84051	N15	π*	0.16837	C16 - C17	17.63
LP (3)	0.74935	O53	σ*	0.06424	N52 - O53	16.51
π	0.83141	C5 - C6	π*	0.27709	N3 - C4	16.33

(b)

Type	Occupancy	Donor atoms (i)	Type	Occupancy	Acceptor atoms (j)	E(2) kcal/ mol
LP (3)	0.7208	O53	π*	0.3683	O51 – N52	121.89
LP*(1)	0.58516	C20	π*	0.26461	C18 - C19	49.14
LP (3)	0.84665	O50	π*	0.36883	O51 - N52	45.35
LP (1)	0.8391	N15	LP*(1)	0.58516	C20	38.74
LP (3)	0.72068	O53	σ*	0.09677	N52 - O53	37.11
LP (1)	0.61194	C30	π*	0.17751	C28 - C29	36.93
LP (1)	0.61194	C30	π*	0.13729	C31 - C32	33.01
LP (3)	0.81966	S2	LP*(6)	0.26892	Zn 1	31.38
LP (3)	0.84762	S14	LP*(6)	0.26892	Zn 1	28.06
π*	0.27445	N3 - C4	π*	0.1274	C5 - C6	26.87
π*	0.1209	C43 - C44	π*	0.0954	C41 - C42	26.32
LP (3)	0.85071	S26	LP*(6)	0.26892	Zn1	23.99
π	0.841	C18 - C19	LP*(1)	0.58516	C20	22.92
LP (3)	0.83843	S38	π*	0.32135	N39 - C40	21.46
LP (2)	0.93101	O50	σ*	0.05618	N3 - H9	21.08
LP (3)	0.84762	S14	LP*(9)	0.08828	Zn1	20.45
π	0.8163	C41 - C42	π*	0.32135	N39 - C40	20.04
π*	0.27445	N3 - C4	π*	0.12673	C7 - C8	19.66
π*	0.32135	N39 - C40	π*	0.0954	C41 - C42	18.1
LP (2)	0.88795	S38	LP*(6)	0.26892	Zn 1	17.93

electron pair occupancy. In the shaded surface maps of Cd and Zn complexes, the vivid red areas signify electron localization (with ELF values ranging between 0.5 and 1.0), while the contrasting blue regions denote electron delocalization (ELF values < 0.5). This visualization aids in comprehending the nuanced electron behavior within these complexes[49].

The elevated regions present in the ELF-shaded surface maps depict the localization of electrons around the hydrogen atom, whereas the blue regions indicate the electron delocalization around carbon and nitrogen atoms. The ELF-shaded surface maps with projections for both complexes are shown in Fig. 7.

ADMET Analysis

The drug-likeness of the novel compounds can be predicted with the aid of Swiss ADME and pkCSM online prediction tools. Further, the properties such as

Table 3 — Various topological properties evaluated at the bond critical points

Compound name	Interactions	ρ_{BCP}	G_{BCP}	V_{BCP}	ε	$\nabla^2\rho_{BCP}$	H_{BCP}	$\|V\|/G$
Cd complex	N3-H9…. O58	0.0126	0.0105	–0.0079	0.0316	0.0522	0.0026	0.7524
Zn complex	N3-H9…. O58	0.0120	0.0091	–0.0071	0.0122	0.0445	0.0020	0.7802

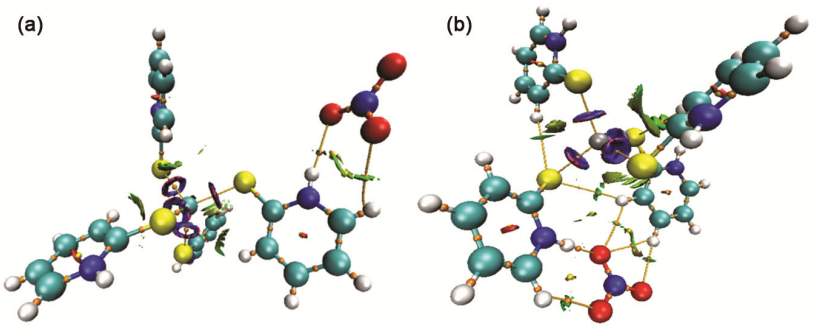

Fig. 5 — The 3D NCI isosurface plots of the (a) Cd complex and (b) Zn complex

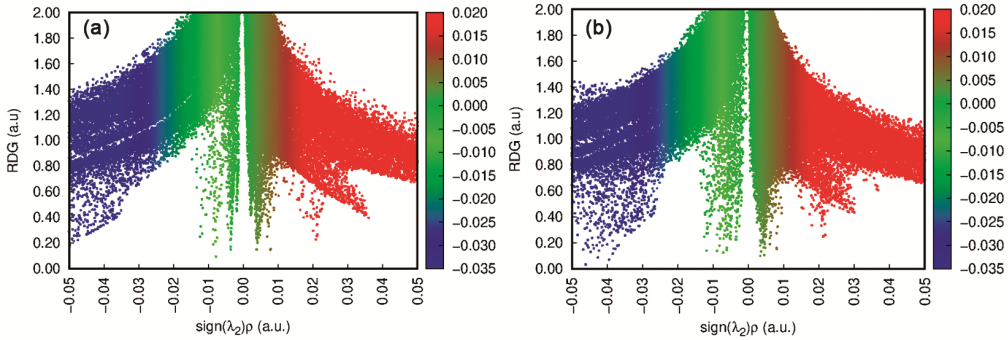

Fig. 6 — The 2D scatter plots of the (a) Cd complex and (b) Zn complex

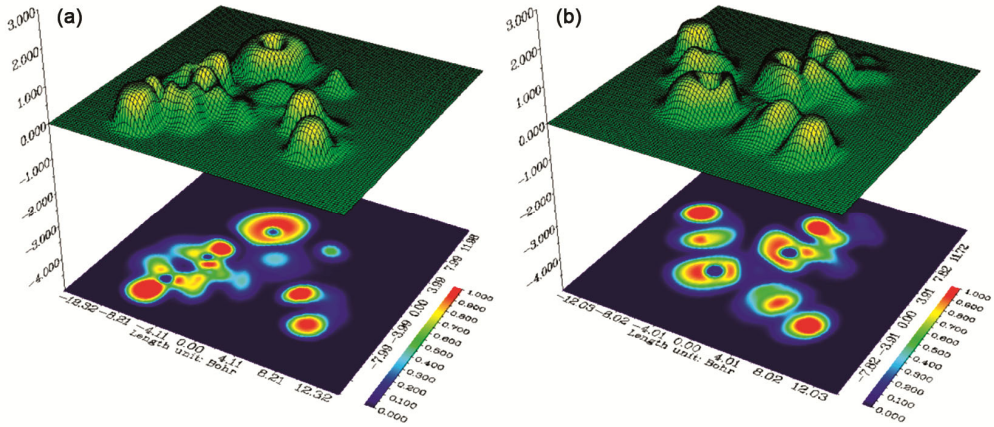

Fig. 7 — The ELF shaded surface map of (a) Cd complex and (b) Zn complex with projection.

metabolism, absorption, excretion, distribution, and toxicity of the novel Cd complex and Zn complex were predicted with the help of pkCSM online tool. The result of this study is shown in Table 4. Both Cd and Zn complex exhibits a very good human intestinal absorption of 96.336%, and 96.384% , respectively. The ADMET analysis revealed that both the compounds showed no toxicity and hepato toxicity. The BOILED - Egg model analysis carried out for both the complexes are shown in the supplementary Fig. S1.

Table 4 — Various ADMET properties of the newly synthesized Cd and Zn complexes, obtained using pkCSM online tool.

Property	Model name	Compound	Predicted value
Absorption	Water solubility (log mol/L)	Cd complex	–5.321
		Zn complex	–5.326
	Caco-2 permeability (log Papp in 10^{-6} cm/s)	Cd complex	0.985
		Zn complex	0.985
	Human intestinal absorption (% absorbed)	Cd complex	96.336
		Zn complex	96.384
	Skin permeability (log Kp)	Cd complex	–2.933
		Zn complex	–2.932
	P-glycoprotein substrate	Cd complex	Yes
		Zn complex	Yes
	P-glycoprotein I inhibitor	Cd complex	Yes
		Zn complex	Yes
	P-glycoprotein II inhibitor	Cd complex	No
		Zn complex	No
Distribution	Human VDss (Log L/kg)	Cd complex	0.151
		Zn complex	0.151
	Fraction unbound (human) (Fu)	Cd complex	0.467
		Zn complex	0.466
	BBB permeability (log BB)	Cd complex	–0.049
		Zn complex	–0.05
	CNS permeability (log PS)	Cd complex	–5.212
		Zn complex	–5.212
Metabolism	CYP2D6 substrate	Cd complex	Yes
		Zn complex	Yes
	CYP3A4 substrate	Cd complex	Yes
		Zn complex	Yes
	CYP1A2 inhibitor	Cd complex	No
		Zn complex	No
	CYP2C19 inhibitor	Cd complex	No
		Zn complex	No
	CYP2C9 inhibitor	Cd complex	No
		Zn complex	No
	CYP2D6 inhibitor	Cd complex	No
		Zn complex	No
	CYP3A4 inhibitor	Cd complex	No
		Zn complex	No
Excretion	Total clearance (log ml/min/kg)	Cd complex	–1.48
		Zn complex	–1.363
	Renal OCT2 substrate	Cd complex	No
		Zn complex	No

(*contd.*)

Table 4 — Various ADMET properties of the newly synthesized Cd and Zn complexes, obtained using pkCSM online tool.

Property	Model name	Compound	Predicted value
Toxicity	AMES toxicity	Cd complex	No
		Zn complex	No
	Maximum tolerated dose (human) (log mg/kg/day)	Cd complex	–0.465
		Zn complex	–0.467
		Cd complex	No
		Zn complex	No
	hERG II inhibitor	Cd complex	Yes
		Zn complex	Yes
	Oral rat acute toxicity (LD50) (mol/kg)	Cd complex	2.955
		Zn complex	2.949
	Oral rat chronic toxicity (LOAEL) (log mg/kg_bw/day)	Cd complex	0.421
		Zn complex	0.421
	Hepatotoxicity	Cd complex	No
		Zn complex	No
	Skin sensitization	Cd complex	No
		Zn complex	No
	T.Pyriformis toxicity (log ug/L)	Cd complex	0.287
		Zn complex	0.287

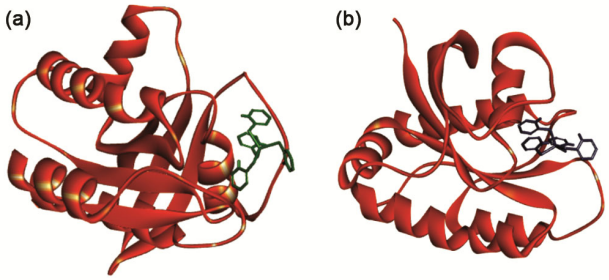

Fig. 8 — Docking pose of (a) Cd and (b) Zn complex against protein PDB ID: 4TQ9

Molecular docking

The interaction of the novel Cd complex and Zn complex with the G12V oncogenic mutant of human GTPase K-Ras protein (PDB ID: 4TQ9) is analyzed with the aid of molecular docking analysis.

The docking analysis showed the binding score of Cd and Zn complex was found to be –7.2 kcal/mol and –7.3 kcal/mol, respectively. The docking poses of the complexes with the protein is given in Fig. 8. The 2D interaction of the complexes with the protein revealed that the amino acids of the protein interact with these complexes through various interactions, such as hydrogen bond, van der Waals, alkyl, π alkyl, and carbon hydrogen bond interactions (Fig. 9). The Cd complex is found to interact with the amino acids ASP30 (2.23 Å), VAL29 (2.84 Å) and LYS117 (3.09 Å) through conventional hydrogen bond interactions. Whereas, for the Zn complex the amino acids LYS117 (4.50 Å) and ASP30 (4.61 Å) interacted through positive-positive and attractive charge interaction respectively. Further, both ASP30 (2.25 Å) and VAL29 (2.86 Å) interacts with the Zn complex *via* hydrogen bond interactions. The 2D interactions of molecular docking of the complexes with the protein moiety are shown in the Fig. 9 (a) and Fig. 9 (b), respectively.

MD simulation analysis

Molecular dynamics provides the insights to see the adaptability and the conformational changes of the compound within the biological system by mimicking the cellular environment and the forces. In the present study, the protein-complex system obtained from the molecular docking was subjected to simulations for a period of 100 ns. Various parameters of the complex such as root mean square fluctuation (RMSF), root mean square deviation (RMSD), protein-ligand contacts, and other properties related to the complex were assessed throughout 100 ns.

In addition to this, the free protein (devoid of the complex) was also exposed to simulations for a period of 100 ns. The comparison was made between the simulation trajectories of the free protein and the protein-complex system. Interestingly, considerable alterations to the protein's orientation associated with the complex were observed. This indicated the variation in the flexibility of the system in both cases.

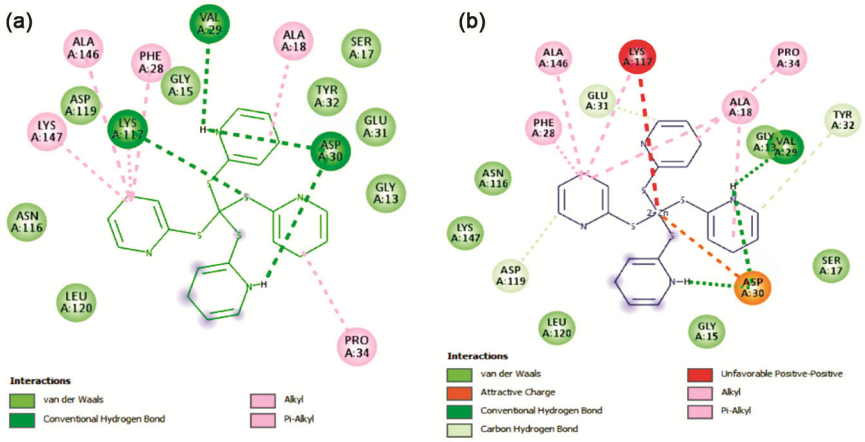

Fig. 9 — 2D interaction plot: (a) Cd and (b) Zn complex when docked against the selected protein

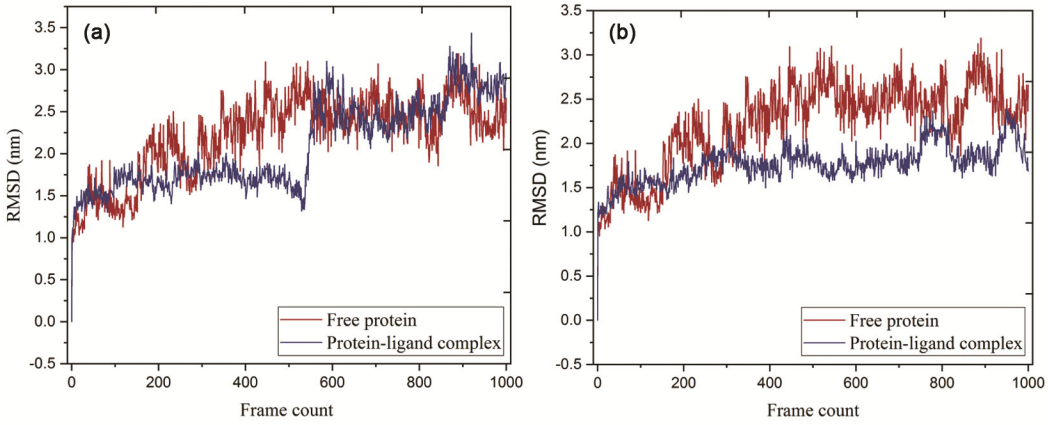

Fig. 10 — RMSD plots of (a) Free protein and protein-Cd complex and (b) Free protein and protein-Zn complex

RMSD analysis

The RMSD plots provide crucial insights into the stability of the protein-complex conformation over time. The main aim of the RMSD analysis in molecular dynamics is to analyze how the conformation of the protein interacting with the complex changes over time to ensure the stability of protein-complex system. The Fig. 10 shows protein-complex system with free protein RMSD plots. The total root mean square deviation plot revealed that the fluctuations of the protein-complex system and free protein are found to be well below 3Å.

The RMSD plots of the protein-Cd complex and protein Zn-complex system associated with the free protein is given in the Fig. 10(a) and Fig. 10(b) respectively. The protein-Zn complex system exhibited superior binding stability in contrast to the protein-Cd complex system. The fluctuations of the protein-Cd system were found to be less compared to that of the free protein upto 60 ns and afterwards a slight increase in the fluctuations was observed.

The RMSD plot of the protein-Zn complex given in the Fig. 11(b) revealed that the fluctuations of the protein-Zn complex is less compared to that of the free protein throughout the simulation time of 100 ns indicating that the protein-Zn complex is stable compared to the free protein. This further indicates that the interaction of the Zn-complex further stabilizes the protein. Further, the fluctuations are found to be less.

Root mean square fluctuations (RMSF)

The RMSF plots reveal the fluctuations of the amino acids during the simulation period and it is helpful in the determination of the flexibility of them in the binding site region. The RMSF plot of the free protein and the protein- Cd (Fig. 11 (a)) and Zn complex system (Fig. 11 (b)) revealed promising results.

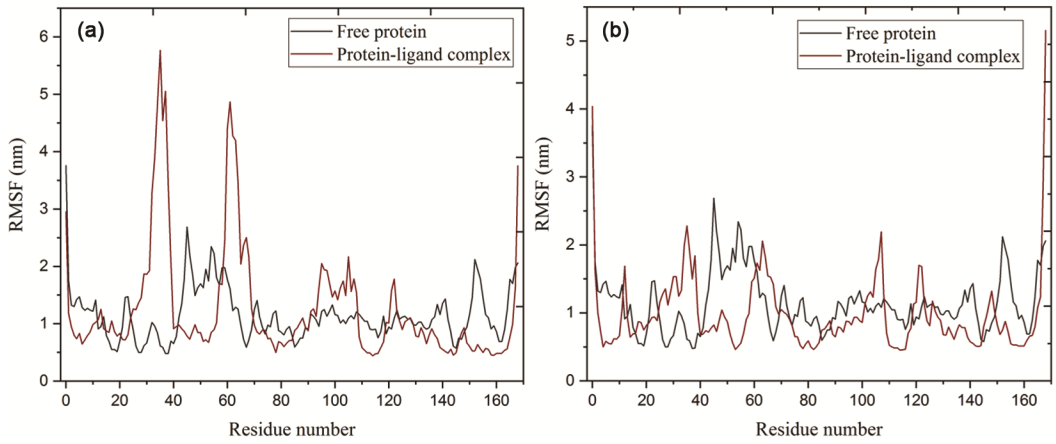

Fig. 11 — The RMSF plots of (a) free protein with protein- Cd complex system and (b) free protein with protein-Zn complex system

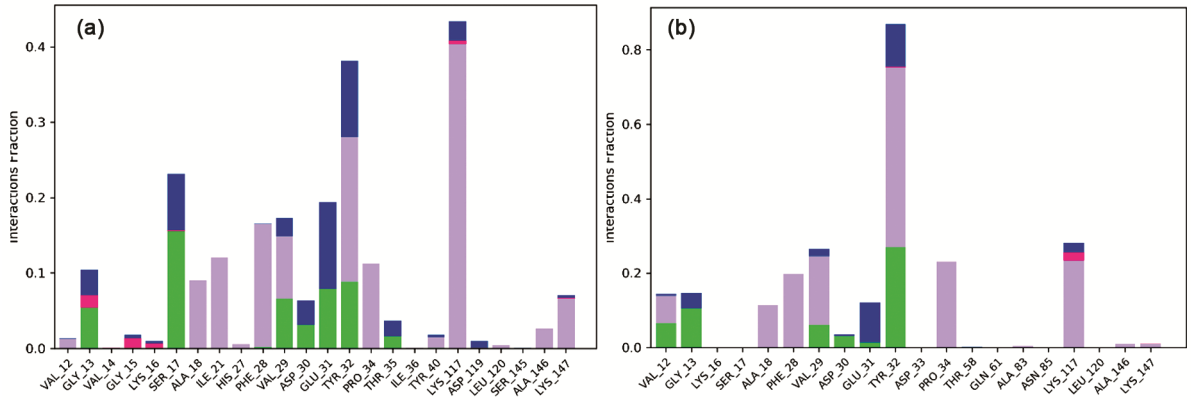

Fig. 12 — The protein-ligand contact (PDBID-4TQ9) map revealing the percentage contribution of the amino acid with the **(a)** Cd complex and **(b)** Zn complex system

The RMSF plot of protein associated with the Cd complex shown in the Fig. 11 (a) revealed that the fluctuations of the amino acids in contact with that of the Cd complex and the amino acids are found to be: ALA156 (5.6 Å), ASP157 (4.8 Å), PHE167 (1.2 Å), VAL178 (1.0 Å), GLU179 (4.28 Å), VAL12 (2.74 Å), GLY13(2.33 Å), PHE28(1.92 Å), SER17 (1.45 Å), LYS117(1.24 Å), TYR32(1.15 Å), LEU120 (2.02 Å), LYS147 (3.24 Å), ILE36 (3.42Å) and ALA146 (1.27 Å) ALA156 (0.52 Å), ASP157 (0.87 Å), PHE167 (0.88 Å), VAL178 (0.45 Å), GLU179 (0.53 Å), MET180 (0.50 Å), GLU181 (0.53 Å), SER203 (0.63 Å), ASP204 (0.63 Å), HIS205 (0.64 Å), ILE206 (0.71 Å), ARG207 (0.86 Å), HIS209 (0.92 Å), GLU210 (0.91 Å), GLN211 (0.82 Å), ARG217 (0.77 Å), and PHE221 (0.60 Å).

Further, the protein-ligand contact map revealed the type of interactions with which these amino acids are interacting with the complex. The protein-Cd complex systems protein-ligand contact map is shown in the Fig. 12 (a). The interactions are categorized and indicated using different colours such as the hydrogen bond interactions with green, hydrophobic with purple colour, ionic and water bridges by pink and blue colour, respectively. The time for which these amino acids interact with the Cd complex is found to be: VAL12(1%), GLY13(4.3%), SER17(16.86%), ALA18(8.3%), ILE21(12.35%), PHE28(16.3%), VAL29(8.3%), ASP30(6.3%), LYS117(38.6%), and LYS147(9.2%) (Fig. 12a).

Further, the fluctuations of the amino acids in contact with the Zn complex is shown in the Fig. 11 (b) and the fluctuations of the amino acids are found to be SER 17 (2.0Å), ASN 85 (2.2Å), VAL12 (1.2Å), GLY13(1.0Å), LYS (1.8Å), TYR32(2.4Å), ASP24(1.86Å), GLN61(1.38Å), ALA86 (2.0 Å), and LEU120 (2.16 Å). The type of interactions exhibited by these amino acids with the complex is found to be: the hydrogen bond interactions were observed between the VAL12 (10.4%), GLY13 (13.2%), TYR32 (21.6%), VAL29 (3.4%), ASP30(4%) and

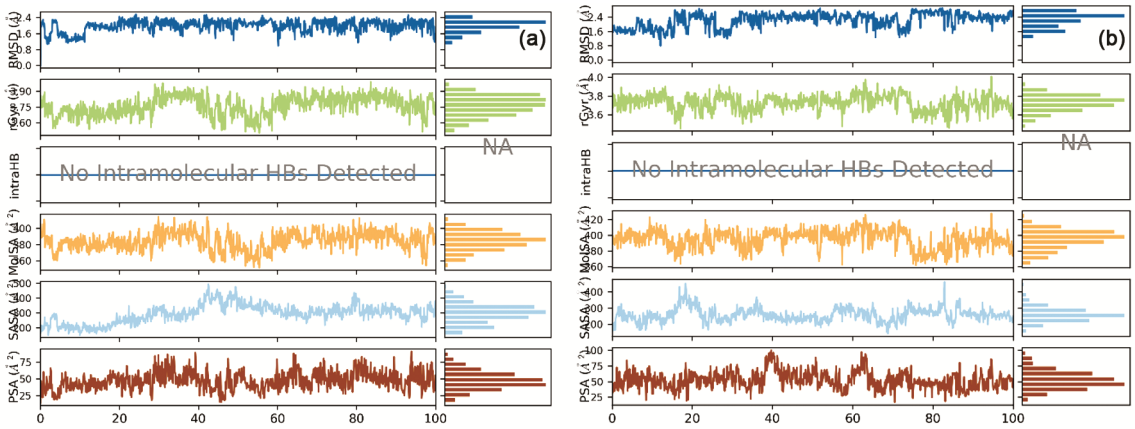

Fig. 13 — Various ligand properties evaluated during the molecular dynamics simulations of the (a) protein-Cd complex and (b) protein-Zn complex systems

GLU31(0.3%) amino acids and the Zn complex. The amino acids VAL12 (7.2%), ALA18 (10.3%), PHE28 (18.6%), VAL29 (18%), TYR32 (53.7%), PRO34 (22.9%) and LYS117 (20.3%) are found to have hydrophobic type of interactions. Further, the amino acids VAL12(0.3%), GLY13 (2.7%), VAL29 (3%), ASP30 (0.4%), GLU31 (11.1%), and TYR32 (12.2%) are found to interact with the Zn complex through the intermediate water molecules (water bridges). Interestingly LYS117(0.36%) exhibited ionic interaction (Fig. 12b).

From the analysis of the RMSD and RMSF plots, the fluctuations of the amino acids in the protein-Zn complex was decreased compared to the free protein, which signifies that the ligand binding has stabilized the fluctuations of the amino acid side chains.

The radius of gyration (rGyr) is a measure used to evaluate the stability of a protein in water, calculated as the common center of mass of the mass-weighted root-mean-square distance of its constituent atoms. The first frame is considered a reference (t=0 ns). Greater stability is indicated by minimal fluctuations in the L-RMSD trajectory, while the radius of gyration gauges the ligand's spread and mirrors its principal moment of inertia. The rGyr indicated that the Cd complex and Zn complex system reached equilibrium at about 2.4 Å.

The other dynamics properties of the protein-complex system such as hydrogen bond, MolSA, SASA and PSA were evaluated. The MoISA, SASA and PSA of Cd complex ranged between 260.38 to 400 Å^2, 200 to 380.18 Å^2 and 25 to 75 Å^2, respectively and the equilibrium was observed at around 380.32 Å^2, 310.49 Å^2 and 52.13 Å^2, respectively. Similarly for Zn complex MoISA, SASA and PSA of Cd complex ranged between 260.13 to 412.62 Å^2, 200.11 to 300.76 Å^2 and 27 to 98 Å^2 and the stability was detected at around 296.88 Å^2, 395.49 Å^2 and 50.36 Å^2 (Fig. 13).

Conclusions

The density functional theory was utilized to conduct geometry optimization for the cadmium and zinc metal complexes. Following this, an assessment of their chemical reactivity and molecular electrostatic potential (MEP) was carried out based on their molecular geometry. The E_{HOMO}-E_{LUMO} energy gap of the alpha and beta spin of both the compounds were found to be similar with cadmium having ΔE value for alpha spin and beta spin to be 0.4414 eV and 3.7462 eV. And for the zinc complex, the value of alpha and beta spins are found to be 0.4860 eV and 3.7345 eV. The highest stabilization energies evaluated for the cadmium and zinc complex evaluated using the NBO analysis were found to be 97.44 kcal/mol and 121.89 kcal/mol, respectively for LP(3)(O53) → π*(C51–N52). Further, the QTAIM-based topology study revealed that for both the complexes $\rho(r)$ and $|V(r)|/\ G(r)$ are found to be < 1 indicating the non-covalent interactions to be weak electrostatic in nature. The small positive values of epsilon and Hermitian evaluated at BCP indicated the delocalization of electrons and closed-shell interactions.

The ADMET analysis revealed that both the cadmium and zinc complexes exhibit no toxicity character and showed very good human intestinal absorption values of 96.336 and 96.384%, respectively. Then both the compounds exhibited a docking score of –7.2 kcal/mol against 4TQ9 protein.

The results from the molecular dynamics analysis indicate that the protein-Zn complex exhibits greater stability than both the free protein and the protein-Cd complex. This suggests that both the cadmium and zinc complexes could serve as promising inhibitors for the 4TQ9 protein.

Acknowledgments

One of the corresponding author (A. Das) would like to extend gratitude for the financial support received from the SERB, DST, GoI, New Delhi (SERB's Sanction order No. EEQ/ 2021/000257 dated 25/02/2022).The authors (Lokanath N. K.; Maithra N. and Chethan B. S.) are thankful to the DST-FIST (SR/FST/PSI-119/2019), University of Mysore, Mysuru for providing the facility.

References

1 Das A, Hussain S A, Banik H, Maiti D, Aktar T, Paul B, Debnath P, Sieron L, Bhattacharya A, Bhowmik K L, Maniukiewicz W & Debnath P, *Polyhedron*, 247 (2024) 116747.
2 Bentabed-Ababsa G, Blanco F, Derdour A, Mongin F, TrécourtF, Quéguiner G, Ballesteros R & Abarca B, *J Org Chem*, 74 (2009) 163.
3 Fujita M, Kwon Y J, Washizu S & Ogura K, *J Am Chem Soc*, 116 (1994) 1151.
4 Habib H A, Hoffmann A, Höppe H A, Steinfeld G & Janiak C, *Inorg Chem*, 48 (2009) 2166.
5 Dong H Z, Zhao J, Gou J S H & Zhu H B, *Polyhedron*, 28 (2009) 1040.
6 Hu T, Liu L, Lv X, Chen X, He H, Dai F, Zhang G & Sun D, *Polyhedron*, 29 (2010) 296.
7 Ronson T K, Adams H, Harding L P, Harrington R W, Clegg W & Ward M W, *Polyhedron*, 26 (2007) 2777.
8 Silva P B D, Frem R C G, Netto A V G, Mauro A E, Ferreira J G & Santos R H A, *Inorg Chem Comm*, 9 (2006) 235.
9 Singh V P, Singh P & Singh A K, *Inorg Chim Acta*, 379 (2011) 56.
10 Mahdavian M & Attar M M, *Corros Sci*, 51 (2009) 409.
11 Durantaye L D L, McCormick T, Liu X Y & Wang S, *Dalton Trans*, 48 (2006) 5675.
12 Janiak C, *Dalton Trans*, 14 (2003) 2781.
13 Millange F, Serre C & Férey G, *Chem Comm*, 8 (2002) 822.
14 Lee K J & Lee T G, *J Hazard Mater*, 241 (2012) 1.
15 Roy S, Bauzá A, Frontera A & Chattopadhyay S, *Inorg Chim Acta*, 450 (2016) 321.
16 Xu Y, Feng L, Jeffrey P D, Shi Y & Morel F M M, *Nature*, 452 (2008) 56.
17 Liguori P F, Valentini A, Palma M, Bellusci A, Bernardini S, Ghedini M, Panno M L, Pettinari C, Marchetti F, Crispini A & Pucci D, *Dalton Trans*, 39 (2010) 4205.
18 Liu S, Cao W, Yu L, Zheng W, Li L, Fan C & Chen T, *Dalton Trans*, 42 (2013) 5932.
19 Modi G, *Der Chem Sin*, 2 (2011) 91.
20 Osowole A A, Ott I & Ogunlana O M, *Int J Inorg Chem*, 2012 (2012) 1.
21 Karmakar T, Kuang Y, Neamati N & Baruah J B, *Polyhedron*, 54 (2013) 285.
22 Li M X, Zhou J, Chen C L & Wang J P, *Z Naturforsch B*, 63 (2008) 280.
23 Fedorov B S, Fadeev M A, Utenyshev A N, Shilov G V, Konovalova N P, Tat'yanenko L V, Sashenkova T E, Blokhina S V & Berseneva E N, *Russ Chem Bull*, 60 (2011) 1959.
24 Strasdeit H, Saak W, Pohl S, Driessen W L & Reedijk J, *Inorg Chem*, 27 (1988) 1557.
25 Jian F F, Zhao P S, Wang Q S & Li Y, *Inorg Chim Acta*, 359 (2006) 1473.
26 Olasunkanmi L O, Obot I B, Kabanda M M & Ebenso E E, *J Phys Chem C*, 119 (2015) 16004.
27 Obot I B & Obi-Egbedi N O, *Mater Chem Phys*, 122 (2010) 325.
28 Fu J, Zang H, Wang Y, Li S, Chen T & Liu X, *Ind Eng Chem Res*, 51 (2012) 6377.
29 Ouali I, Hammouti B, Aouniti A, Ramli Y, Azougagh M, Essassi E M & Bouachrine M, *J Mat Env Sci*, 1 (2010) 1.
30 Dennington R, Keith TA & Millam J M, *Gauss View, Version 6.0. 16*, (Semichem Inc Shawnee Mission KS), 2016.
31 Frisch M J, Trucks G W, Schlegel H B, Scuseria G E, Robb M A, Cheeseman J R, Scalmani G, Barone V, Petersson G A & Nakatsuji H, *Gaussian 16*, (Gaussian, Inc.: Wallingford, CT, USA) 2016.
32 Frisch M J, Trucks G W, Schlegel H B, Scuseria G E, Robb M A, Cheeseman J R, Scalmani G, Barone V, Petersson G A & Nakatsuji H, *Gaussian 16*, (Gaussian, Inc. Wallingford, CT) 2016.
33 Humphrey W, Dalke A & Schulten K, *J Mol Graph*, 14 (1996) 33.
34 Daina A, Michielin O & Zoete V, *Sci Rep*, 7 (2017) 42717.
35 Pires D E, Blundell T L & Ascher D B, *J Med Chem*, 58 (2015) 4066.
36 Herrmann D & Thomas W, *J Int Acc Audit Tax*, 5 (1996) 1.
37 Milburn MV, Tong L, DeVos A M, Brünger A, Yamaizumi Z, Nishimura S & Kim S H, *Science*, 247 (1990) 939.
38 Vetter I R & Wittinghofer A, *Science*, 294 (2001) 1299.
39 Vatansever S, Erman B & Gümüş Z H, *Comp Struc Biotech J*, 18 (2020) 1000.
40 Pantsar T, Rissanen S, Dauch D, Laitinen T, Vattulainen I & Poso A, *Comp Bio*, 14 (2018) e1006458.
41 Lu S, Jang H, Nussinov R & Zhang J, *Sci Rep*, 6 (2016) 2194.
42 Biovia D S, *Discovery Studio Modeling Environment*, Release, 2017.
43 Morris G M, Huey R, Lindstrom W, Sanner M F, Belew R K, Goodsell D S & Olson A J, *J Comp Chem*, 30 (2009) 2785.
44 Trott O, Olson A J, *J Comp Chem*, 31 (2010) 455.
45 Huey R, Morris G M & Forli S, *Scripps Res Inst Mole Graph Lab*, 10550 (2012) 1000.
46 Jamkhande P G, Ghante M H & Ajgunde B R, *Bull Fac Pharm Cairo Univ*, 55 (2017) 203.
47 Nanjundaswamy S, Gurumallappa, Hema M K, Karthik C S, Rajabathar J R, Arokiyaraj S, Lokanath N K & Mallu P, *J Mol Struct*, 1247 (2022) 131365.
48 Nagaraju M, Karthik C S, Hema M K, Chethan B S, Ramalingam R J, Karnan M & Lokanath N K, *J Biomol Struct Dyn*, (2023) 1.
49 Savin A, Nesper R, Wengert S & Fässler T F, *Angew Chem Int Ed Engl*, 36 (1997) 1808.